ACS Macro Letters
Letter
pubs.acs.org/macroletters

Structure and Strength at Immiscible Polymer Interfaces

Ting Ge,[†] Gary S. Grest,[‡] and Mark O. Robbins*,[†]

[†]Department of Physics and Astronomy, Johns Hopkins University, Baltimore, Maryland 21218, United States
[‡]Sandia National Laboratories, Albuquerque, New Mexico 87185, United States

Ⓢ *Supporting Information*

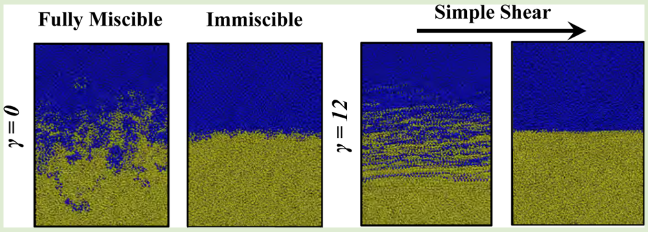

ABSTRACT: Thermal welding of polymer−polymer interfaces is important for integrating polymeric elements into devices. When two different polymers are joined, the strength of the weld depends critically on the degree of immiscibility. We perform large-scale molecular dynamics simulations of the structure−strength relation at immiscible polymer interfaces. Our simulations show that immiscibility arrests interdiffusion and limits the equilibrium interfacial width. Even for weakly immiscible films, the narrow interface is unable to transfer stress upon deformation as effectively as the bulk material, and chain pullout at the interface becomes the dominant failure mechanism. This greatly reduces the interfacial strength. The weak response of immiscible interfaces is shown to arise from an insufficient density of entanglements across the interface. We demonstrate that there is a threshold interfacial width below which no significant entanglements can form between opposite sides to strengthen the interface.

Disparate polymers usually do not mix well.[1−4] As even a small energy penalty associated with contact of different constituent monomers is amplified by the high degree of polymerization, the enthalpic contribution to the free energy often dominates over the entropy gain due to partial mixing. As a result, an equilibrium interface of limited width forms between immiscible polymers. This type of interface exists in numerous applications of polymer blends[4] and exhibits low mechanical strength during large deformation and fracture.[5,6] An understanding of the molecular origin of this weakness may aid development of novel techniques for reinforcing immiscible polymer interfaces.

Computer simulations access molecular details that are difficult to observe in experiments and thus provide unique insight into interfacial structure and mechanical processes. In particular, recently developed algorithms[7−9] have enabled simulations to track entanglements on a microscopic level. The entanglement density can be directly related to the viscoelastic response of high molecular weight polymer melts.[3,10,11] Experiments have suggested that entanglements strongly affect the mechanical properties of interfaces between glassy polymers,[5,12−17] and many theoretical models also assume that entanglements play a critical role.[5,18−20]

In this Letter, we present results from large-scale molecular dynamics (MD) simulations of the interdiffusion between highly entangled immiscible polymers. As the degree of immiscibility increases, the equilibrium interfacial width decreases and is reached at an earlier interdiffusion time t. The interfacial strength of an immiscible interface is always lower than that of a fully miscible interface at the same t and saturates below the bulk strength in equilibrium. Immiscible interfaces are not able to transfer stress effectively because chains can pull out from the opposing surface, while failure of bulk systems requires chain scission. We use the Primitive Path Analysis (PPA) algorithm[7,21] to identify entanglements and correlate them with mechanical response. Entanglement densities are greatly reduced at immiscible interfaces relative to bulk values and we find that no entanglements form across the interface for interdiffusion depths below a threshold value.

All of the simulations employed the canonical bead−spring model[22] that captures the properties of linear homopolymers. The van der Waals interactions between like monomers of mass m are modeled using the standard Lennard-Jones potential with interaction strength u_0, diameter a, and characteristic time $\tau = a(m/u_0)^{1/2}$. To model immiscible films, the interaction strength u_0 between unlike monomers was reduced to $\tilde{\varepsilon}_{12}u_0 < u_0$. Here we simulated four systems with $\tilde{\varepsilon}_{12} = 1.0, 0.99, 0.98$, and 0.95.

Chains of length $N = 500$ beads were made by coupling nearest-neighbors with an additional potential. Because chain scission plays an essential role in the mechanical tests, the usual unbreakable finitely extensible nonlinear elastic (FENE) potential[22] was replaced by a simple quartic potential with the same equilibrium spacing and a breaking force of $240u_0/a$. This is 100 times higher than the maximum attractive force for the Lennard-Jones potential, which is consistent with experiments and previous simulations.[23−25] Previous work has shown that the entanglement length for this model is $N_e = 85 \pm 7$ and that the mechanical response for $N = 500$ is characteristic of highly entangled (large N) polymers.[23,26−29] Further simulation details can be found in the Supporting Information.

Fluid films of each polymer species were equilibrated separately at temperature $T = 1.0u_0/k_B$. Each film contains

Received: August 4, 2013
Accepted: September 12, 2013
Published: September 19, 2013

dx.doi.org/10.1021/mz400407m | *ACS Macro Lett.* 2013, 2, 882−886

2.4 million beads in $M = 4800$ chains. Periodic boundary conditions were applied along the x- and y-directions with dimensions $L_x = 700a$ and $L_y = 40a$, while featureless walls separated by $L_z = 100a$ confined films in the nonperiodic z-direction. Equilibrated films were placed in contact and allowed to interdiffuse for a time t. The system was then quenched rapidly to $T = 0.2u_0/k_B$, which is below the glass temperature $T_g \approx 0.35u_0/k_B$.[30] To test mechanical strength, shear was applied to the glassy interface in a manner similar to a shear test of a lap joint in experiments[5] and recent simulations.[25] Interfaces for different $\tilde{\varepsilon}_{12}$ before and after shearing are visualized in Figure 1.

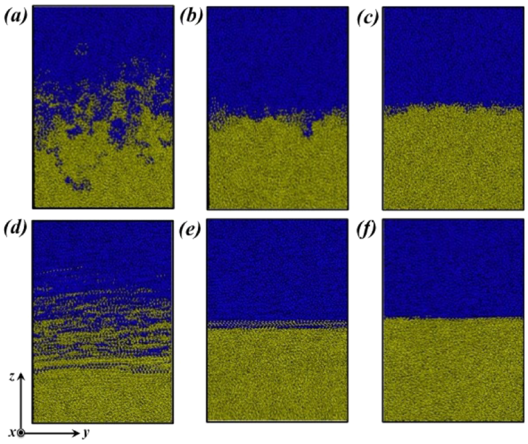

Figure 1. Snapshots of the interface between thin polymer films of types 1 (yellow) and 2 (blue) at $T = 0.2u_0/k_B$ before deformation (top) and at a large shear strain $\gamma = 12$ (bottom). Snapshots (a, d) are for a fully miscible interface ($\tilde{\varepsilon}_{12} = 1.0$) at interdiffusion time $t = 5M\tau$, (b, e) and (c, f) show equilibrium states for $\tilde{\varepsilon}_{12} = 0.99$ and 0.95, respectively. For clarity, only a portion of the sample is shown: $40a$ along the direction of shear (y) and $60a$ in the velocity gradient direction (z).

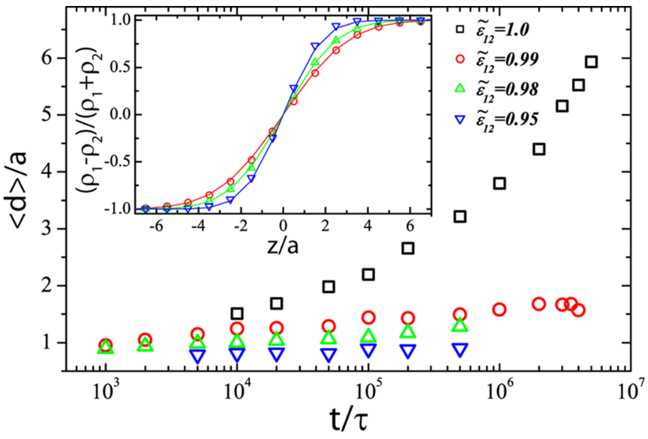

Figure 2. Average interdiffusion depth $\langle d\rangle$ of monomers across the interface as a function of t for different $\tilde{\varepsilon}_{12}$. The inset shows the normalized density difference profile for immiscible interfaces at equilibrium. Solid lines show fits to an error function $\mathrm{erf}(\pi^{1/2}z/w)$.

Figure 2 shows the average interdiffusion depth $\langle d\rangle$ of monomers across the interface as a function of time t for different $\tilde{\varepsilon}_{12}$. For monomers of type 1 that are below the initial interface ($z = 0$), $\langle d\rangle \equiv \int_0^{+\infty}(z)\rho_1(z)\mathrm{d}z/\int_0^{+\infty}\rho_1(z)\mathrm{d}z$, where $\rho_1(z)$ is number density. For monomers of type 2, the integration range is changed to $z < 0$. The depth keeps rising with t for $\tilde{\varepsilon}_{12} = 1.0$, because interdiffusion between fully miscible polymers is a kinetic process that continues indefinitely. In contrast, for $\tilde{\varepsilon}_{12} = 0.99$, $\langle d\rangle$ increases slowly with t and reaches a plateau when the entropy gained from mixing is balanced by the energetic penalty. We use the states at $t = 4M\tau$, $0.5M\tau$, and $0.5M\tau$ ($1M\tau = 10^6\tau$) to represent the equilibrium interface for $\tilde{\varepsilon}_{12} = 0.99$, 0.98, and 0.95, respectively. The corresponding plateau values of $\langle d\rangle$ are about $1.6a$, $1.3a$, and $0.9a$. All are much smaller than the width for $\tilde{\varepsilon}_{12} = 1.0$ at the same times.

Separate simulations[31,32] of the self-diffusion of polymer chains with $N = 500$ in bulk melts find that the entanglement time $\tau_e \sim 10^4\ \tau$, while the disentanglement time $\tau_d \sim 30M\tau$. However, one needs to be careful when comparing the times for interdiffusion with the characteristic times (τ_e and τ_d) for self-diffusion, because the interdiffusion at early times is found to be dominated by the motion of chain ends,[31] and also, in this study, the interdiffusion is affected by the immiscibility.

The reduction of interfacial width due to increasing immiscibility is illustrated by snapshots in Figure 1a−c. Note that a 1% decrease of $\tilde{\varepsilon}_{12}$ from 1.0 to 0.99 already leads to a narrow interface with a finite $\langle d\rangle$. The sensitivity of interfacial structure to a slight dissimilarity between unlike monomers is well captured by our simulation.

The equilibrium interface width of immiscible polymers is often quantified by the concentration profile.[5,6] The inset of Figure 2 shows $(\rho_1(z) - \rho_2(z))/(\rho_1(z) + \rho_2(z))$. Solid lines are results from fitting the data points using the error function $\mathrm{erf}(\sqrt{\pi}z/w)$.[33] Here $w = 4\langle d\rangle$ characterizes the equilibrium interfacial width. Measured values of w are consistent with $4\langle d\rangle$ ($w = 6.13 \pm 0.04a$, $4.98 \pm 0.04a$, and $3.63 \pm 0.04a$ for $\tilde{\varepsilon}_{12} = 0.99$, 0.98, and 0.95, respectively). Helfand and Tagami argued that the width should be twice the radius of gyration of the chain segments that penetrated across the interface, and that these should have length $1/\chi$, where χ is the phenomenological Flory interaction parameter. Then $w \sim 2[l_K l_0/6\chi]^{1/2}$, where $l_K = 1.77a$ is the Kuhn length and $l_0 = 0.96a$ the bond length. In our model, χ scales with $(1 - \tilde{\varepsilon}_{12})$, but the exact mapping between them is not clear. While this prevents us from testing Helfand and Tagami's expression, we can use it to estimate that $\chi = 0.030$, 0.046, and 0.086 for $\tilde{\varepsilon}_{12} = 0.99$, 0.98, and 0.95, respectively.

Figure 3a illustrates how the reduced interfacial width changes stress−strain curves from the bulk response, which is the same for both species. All stress curves show nearly the same initial regimes of linear elastic response, yield, and strain hardening as the shear strain γ increases. For $t > 4M\tau$ the response for $\tilde{\varepsilon}_{12} = 1.0$ is indistinguishable from the average bulk result even though polymers have diffused by much less than their radius of gyration.[25] As $\tilde{\varepsilon}_{12}$ decreases, the stress drops below the bulk response at progressively earlier strains. Greater immiscibility also lowers the peak stress $\sigma_{\max}$ where failure occurs.

As in experiment,[5] we use $\sigma_{\max}$ to characterize the interfacial strength. Figure 3b shows $\sigma_{\max}$ normalized by the average bulk failure stress $\sigma_{\max}^{\mathrm{bulk}}$ versus time t for different $\tilde{\varepsilon}_{12}$. For $\tilde{\varepsilon}_{12} = 1.0$, the bulk strength is recovered by approximately $4M\tau$. For $\tilde{\varepsilon}_{12} = 0.99$, the development of $\sigma_{\max}$ is delayed and starts to rise around $0.2M\tau$. Ultimately, it reaches a plateau value that is about one-half of $\sigma_{\max}^{\mathrm{bulk}}$. For $\tilde{\varepsilon}_{12} = 0.98$ and 0.95, there is almost no change in $\sigma_{\max}$ with the interdiffusion time t, and $\sigma_{\max}$ remains at a lower value. Similar reductions in the strength of interfaces between two immiscible polymers have been observed in experiments.[5]

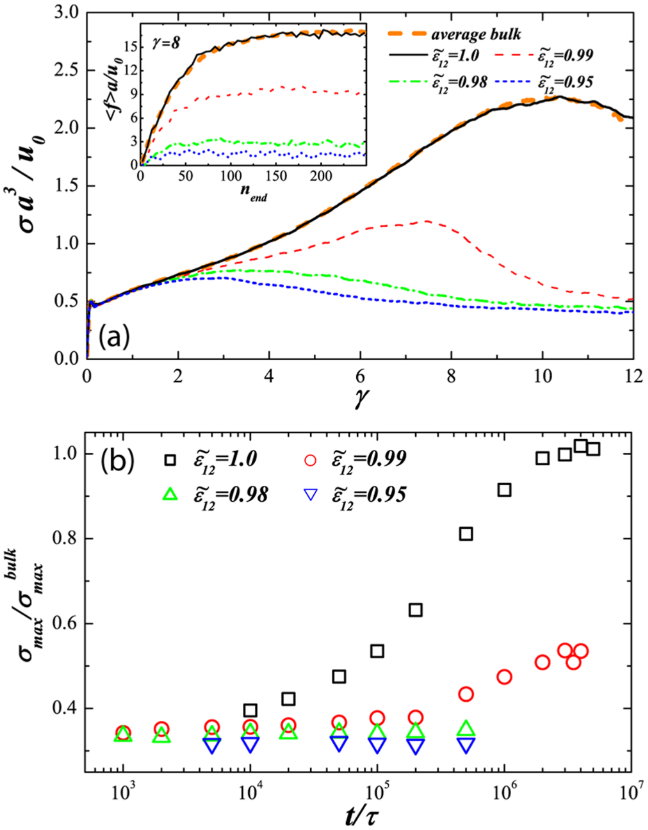

Figure 3. (a) Stress−strain curves from shear tests on the fully miscible interface at $t = 5M\tau$ and immiscible interfaces at equilibrium. Also shown is the average bulk result. The inset shows the corresponding average bond tension $\langle f\rangle$ as a function of the distance in monomers n_{end} from the nearest chain end for $\gamma = 8$. (b) The maximum shear stress $\sigma_{\max}$ before failure normalized by the average bulk value $\sigma_{\max}^{\mathrm{bulk}}$ as a function of t.

Simulations allow us to directly follow the evolution of interfacial structure during shearing and to determine the failure mechanism. Previous simulations[25] revealed that bulk systems fail through chain scission. The same mechanism occurs at long t for $\tilde{\varepsilon}_{12} = 1.0$, and the fact that broken bonds are spread uniformly through the sample rather than near the interface confirms that the interface is as strong as the bulk for $t \geq 4M\tau$. Figure 1d illustrates the distribution of monomers at $\gamma = 12$ for this limit. The chain segments that have diffused across the interface become highly oriented during shearing, but have been broken off and continue to shear with the opposing film.

Immiscible interfaces with $\tilde{\varepsilon}_{12} = 0.95$ and 0.98 fail through chain pullout at the interface. As illustrated in Figure 1f for $\tilde{\varepsilon}_{12} = 0.95$, there is a sharp interface at $\gamma = 12$ with all chain segments pulled out from the opposing film. The same mechanism is observed for $\tilde{\varepsilon}_{12} = 1.0$ at short welding times. For $\tilde{\varepsilon}_{12} = 0.99$, the failure mechanism is beginning to crossover from chain pullout to chain scission. However, as shown in Figure 1e, only a tiny fraction of monomers remain in the opposite side at $\gamma = 12$ and the rest have have been pulled out. Bonds that have broken by $\gamma = 12$ are predominantly distributed near the interface, indicating that it is mechanically weaker than the surrounding bulk regions.

These changes in failure mechanism are directly correlated with the rise in tension along backbone bonds that accompanies strain hardening at large strains.[28] The inset in Figure 3a shows the mean bond tension $\langle f\rangle$ as a function of the number of bonds n_{end} to the nearest chain end. Results are shown for $\gamma = 8$, where the results for $\tilde{\varepsilon}_{12} = 0.95$ and 0.98 have saturated and the rate of bond breaking is fastest for $\tilde{\varepsilon}_{12} = 0.99$ and 1.0. The curves can be fit to $\langle f\rangle = f_0(1 - \exp(-n_{\mathrm{end}}/n_{\mathrm{end}}^{\mathrm{c}}))$, where f_0 corresponds to the plateau tension far from ends, and $n_{\mathrm{end}}^{\mathrm{c}}$ is the characteristic distance for tension relaxation near chain ends. For $\tilde{\varepsilon}_{12} = 1.0$, the whole distribution of $\langle f\rangle$ overlaps with that in the bulk, consistent with the results for the stress−strain behavior. The length near the end where stress has relaxed, $n_{\mathrm{end}}^{\mathrm{c}}$, is only about half N_e and much smaller than the length of chain segments that have diffused across the interface. While f_0 is substantially smaller than the force for chain scission, there is a long tail in the distribution that decays exponentially with a characteristic decay force equal to f_0.[26] This allows enough chain scission to produce failure, about 1 in 10^4 bonds at any time. As immiscibility increases, the maximum f_0 decreases until there is negligible scission. The value of $n_{\mathrm{end}}^{\mathrm{c}}$ also decreases, with $n_{\mathrm{end}}^{\mathrm{c}} = 42 \pm 2$, 33 ± 2, 21 ± 2, and 13 ± 3 for $\tilde{\varepsilon}_{12} = 1.0$, 0.99, 0.98, and 0.95, respectively. End segments with length of order $n_{\mathrm{end}}^{\mathrm{c}}$ can pullout from their confining tubes. We find the length in beads n^* of segments that diffuse across the interface is very close to $n_{\mathrm{end}}^{\mathrm{c}}$ for systems that fail by chain pullout: 33, 22, and 12 for $\tilde{\varepsilon}_{12} = 0.99$, 0.98, and 0.95, respectively. These lengths are obtained using Helfand and Tagami's estimate that $w/2$ corresponds to the radius of gyration of chains of length n^*. Experiments have also observed chain pullout at weak immiscible polymer interfaces.[5,13,15]

Our previous study of miscible interfaces[25] showed that entanglements between chains from opposite sides of the interface were required to prevent chain pullout and lead to chain scission. One would expect that chain pullout at immiscible interfaces also results from a lack of interfacial entanglements. To test this idea, we tracked entanglements using the PPA, which identifies entanglements as binary contacts between the underlying primitive paths of polymer chains. PPA has provided unique insights into properties of entangled polymer melts,[7−9] because entanglements have remained elusive objects in experimental studies.

In PPA, the primitive paths are revealed by fixing the chain ends and minimizing the chain length without allowing chain crossing. To limit excluded volume effects, the chain diameter is then reduced by a factor of 4 and additional monomers introduced to prevent chain crossing.[21] Contacts between the resulting primitive paths are counted to determine the number of topological constraints (TCs). We find that the ratio of the density of TCs, ρ_{TC}, to the bulk density, $\rho_{\mathrm{TC}}^{\mathrm{bulk}}$, is insensitive to the procedural details in identifying the TCs. Past studies on bulk polymers have shown that ρ_{TC} is proportional to the entanglement density,[7−9,21] and we refer to TCs and entanglements interchangeably below.

Figure 4a shows the profile of $\rho_{\mathrm{TC}}(z)/\rho_{\mathrm{TC}}^{\mathrm{bulk}}$ for the same interfaces shown in Figure 3. For $\tilde{\varepsilon}_{12} = 1.0$, the bulk entanglement density is recovered across the interface at $t \geq 4M\tau$, when the bulk mechanical response has also been recovered. For $\tilde{\varepsilon}_{12} < 1.0$, the density of entanglements is greatly reduced at the interface. $\rho_{\mathrm{TC}}(z)$ is very small near the interface for $\tilde{\varepsilon}_{12} = 0.99$ and 0.98 and is essentially nonexistent for $\tilde{\varepsilon}_{12} = 0.95$. This trend correlates with the reduction of interfacial strength as immiscibility increases.

The distributions of TCs for immiscible interfaces exhibit two peaks on either side of the interface. This reflects the anisotropic conformation of chains, which are compressed normal to the free surface before interdiffusion.[34−36] Chains

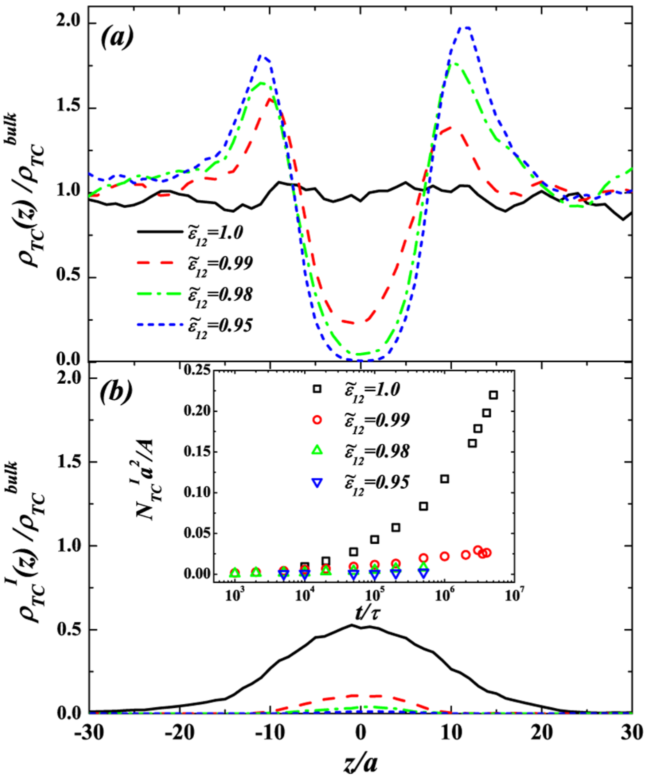

Figure 4. Density profiles of (a) all and (b) interfacial TCs for the same interfaces shown in Figure 3. Results are normalized by the bulk density of TCs. The inset of (b) shows the areal density of interfacial TCs, N^{I}_{TC}/A vs t.

with pancake-like conformations near the interface are subject to more TCs. Because immiscibility limits the interdiffusion, these chains cannot relax to their isotropic conformation as in the miscible case. As a result, the peaks in $\rho_{TC}(z)$ at the interface are preserved at equilibrium. Note that the position of the peak in TC density may be shifted by the PPA, which introduces a tension to shorten chain contour lengths that may move TCs toward places with higher density. However the changes in density with time and the total number of interfacial TCs are not sensitive to such shifts.

Interfacial entanglements between chains from two different sides are crucial to anchoring chain segments to the opposite side. The distributions of these interfacial entanglements are shown in Figure 4b. The inset of Figure 4b shows how immiscibility arrests the formation of interfacial entanglements. The areal density of interfacial TCs, N^{I}_{TC}/A, is plotted against t for the four values of $\tilde{\varepsilon}_{12}$. For $\tilde{\varepsilon}_{12}$ = 1.0, N^{I}_{TC}/A continues to increase with interdiffusion time. When chains have formed 2–3 interfacial entanglements, chain pullout is suppressed and bulk strength is achieved.[25] For $\tilde{\varepsilon}_{12}$ = 0.99, the number of interfacial entanglements is greatly suppressed, while for $\tilde{\varepsilon}_{12}$ = 0.98 and 0.95, there are almost no interfacial entanglements.

Experiments do not provide a direct measurement of entanglements and the interfacial width has often been used as an indirect measure.[12−14,16] Our simulations allow us to quantify the relation between N_{TC}/A and $\langle d\rangle$. Figure 5 shows that results for different $\tilde{\varepsilon}_{12}$ are consistent with a common curve. At large widths, N^{I}_{TC}/A rises linearly with $\langle d\rangle$. We have shown that this agrees with a scaling prediction based on the chain-packing model.[25] The linear region extrapolates to N^{I}_{TC} = 0 at $\langle d\rangle \sim 1.5a$, and the density of entanglements is nearly zero

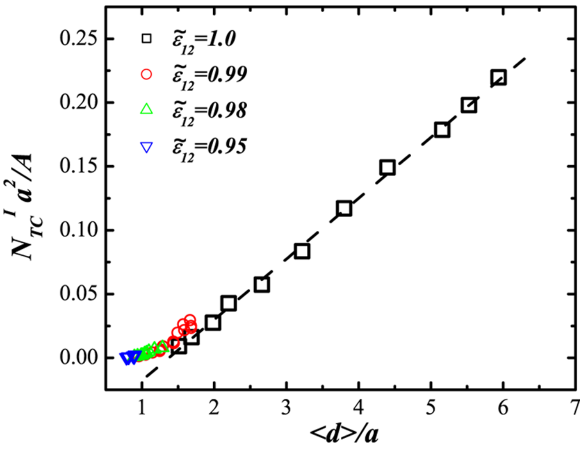

Figure 5. Areal density of interfacial TCs, N^{I}_{TC}/A, vs the average interdiffusion depth $\langle d\rangle$. Dashed line is the linear fit for the fully miscible case.

for widths below this threshold value. For $\tilde{\varepsilon}_{12}$ = 0.99 the width rises above this threshold and a slight upturn in entanglement density starts near $\langle d\rangle$ = 1.5. For less miscible systems $\langle d\rangle$ remains below 1.5a and almost no entanglements form. De Gennes[18] argued that the probability of entanglements across an immiscible interface at equilibrium should scale as $\exp(-N_e\chi)$, reflecting the probability for a loop crossing the interface having length larger than N_e. This is qualitatively consistent with the loop statistics we measure (Figure 1 in the Supporting Information) and explains the rapid drop in entanglements as $\tilde{\varepsilon}_{12}$ decreases. Given $N_e \sim 85$ and our estimates of χ, $\exp(-N_e\chi)$ = 0.08, 0.02, and 0.0007 for $\tilde{\varepsilon}_{12}$ = 0.99, 0.98, and 0.95, respectively.

There is a strong correlation between the threshold width for entanglement formation and interfacial shear strength. Comparing Figure 2 and Figure 3b, we see that there is a sharp rise in σ_{max} at the time when $\langle d\rangle$ exceeds 1.5a for $\tilde{\varepsilon}_{12}$ = 1.0 and 0.99. Less miscible systems show little increase in strength because $\langle d\rangle$ remains below the threshold value. Experiments have also found that a minimum interfacial width is needed for the development of interfacial strength.[12,13] One way of broadening interfaces in such immiscible systems is to add random copolymers, and experiments show this is effective in raising interfacial strength.[15] This will be an interesting topic for future simulation studies.

To summarize, we have demonstrated that the mechanical weakness of immiscible polymer interfaces is closely related to the lack of entanglements at the interface. The development of entanglements is greatly suppressed due to limited interdiffusion. At equilibrium, the density of entanglements is reduced compared to that in the bulk. Consequently, chains can be easily pulled out from the opposite side at a low stress. Our results also show that there is a minimum interdiffusion depth required for significant entanglement formation and therefore growth of the interfacial strength. These findings should help further development of theoretical descriptions of entanglement formation and fracture behavior at immiscible polymer–polymer interfaces, and also benefit engineering design of interfacial strengthening mechanisms.

■ ASSOCIATED CONTENT

Ⓢ Supporting Information

Simulation details. This material is available free of charge via the Internet at http://pubs.acs.org.

■ AUTHOR INFORMATION

Corresponding Author

*E-mail: mr@jhu.edu.

Notes

The authors declare no competing financial interest.

■ ACKNOWLEDGMENTS

This work was supported in part by the National Science Foundation under Grant Nos. DMR-1006805, CMMI-0923018, and OCI-0963185. M.O.R. acknowledges support from the Simons Foundation. This research used resources at the National Energy Research Scientific Computing Center, which is supported by the Office of Science of the United States Department of Energy under Contract No. DE-AC02-05CH11231. Research was carried out in part at the Center for Integrated Nanotechnologies, a U.S. Department of Energy, Office of Basic Energy Sciences, user facility. Sandia National Laboratories is a multiprogram laboratory managed and operated by Sandia Corporation, a wholly owned subsidiary of Lockheed Martin Corporation, for the U.S. Department of Energy's National Nuclear Security Administration under Contract No. DE-AC04-94AL85000.

■ REFERENCES

(1) Helfand, E.; Tagami, Y. *J. Polym. Sci., Part B: Polym. Phys.* **1971**, *9*, 741−746.

(2) Helfand, E.; Tagami, Y. *J. Chem. Phys.* **1972**, *56*, 3592−3601.

(3) Rubinstein, M.; Colby, R. H. *Polymer Physics*; Oxford University Press: Oxford, 2003.

(4) Robeson, L. M. *Polymer Blends: A Comprehensive Review*; Hanser-Gardner Publications: Cincinnati, OH, 2007.

(5) Wool, R. P. *Polymer Interfaces: Structure and Strength*; Hanser: Munich, 1995.

(6) Jones, R. A. L.; Richards, R. W. *Polymers at Surfaces and Interfaces*; Cambridge University Press: New York, 1999.

(7) Everaers, R.; Sukumaran, S. K.; Grest, G. S.; Svaneborg, C.; Sivasubramanian, A.; Kremer, K. *Science* **2004**, *303*, 823−826.

(8) Kröger, M. *Comput. Phys. Commun.* **2005**, *168*, 209−232.

(9) Tzoumanekas, C.; Theodorou, D. N. *Macromolecules* **2006**, *39*, 4592−4604.

(10) de Gennes, P. G. *J. Chem. Phys.* **1971**, *55*, 572−579.

(11) Doi, M.; Edwards, S. F. *The Theory of Polymer Dynamics*; Oxford University Press: Oxford, 1988.

(12) Schnell, R.; Stamm, M.; Creton, C. *Macromolecules* **1998**, *31*, 2284−2292.

(13) Schnell, R.; Stamm, M.; Creton, C. *Macromolecules* **1999**, *32*, 3420−3425.

(14) Brown, H. R. *Macromolecules* **2001**, *34*, 3720−3724.

(15) Creton, C.; Kramer, E. J.; Brown, H. R.; Hui, C.-Y. *Adv. Polym. Sci.* **2001**, *156*, 53−136.

(16) Cole, P. J.; Cook, R. F.; Macosko, C. W. *Macromolecules* **2003**, *36*, 2808−2815.

(17) Boiko, Y. M. *Colloid Polym. Sci.* **2012**, *290*, 1201−1206.

(18) de Gennes, P. G. *C. R. Acad. Sci., Ser. II* **1989**, *308*, 1401−1403.

(19) Benkoski, J. J.; Fredrickson, G. H.; Kramer, E. J. *J. Polym. Sci., Part B: Polym. Phys.* **2002**, *40*, 2377−2386.

(20) Silvestri, L.; Brown, H. R.; Carra, S.; Carra, S. *J. Chem. Phys.* **2003**, *119*, 8140−8149.

(21) Hoy, R. S.; Grest, G. S. *Macromolecules* **2007**, *40*, 8389−8395.

(22) Kremer, K.; Grest, G. S. *J. Chem. Phys.* **1990**, *92*, 5057−5086.

(23) Rottler, J.; Barsky, S.; Robbins, M. O. *Phys. Rev. Lett.* **2002**, *89*, 148304.

(24) Stevens, M. J. *Macromolecules* **2001**, *34*, 2710−2718.

(25) Ge, T.; Pierce, F.; Perahia, D.; Grest, G. S.; Robbins, M. O. *Phys. Rev. Lett.* **2013**, *110*, 98301.

(26) Rottler, J.; Robbins, M. O. *Phys. Rev. Lett.* **2002**, *89*, 195501.

(27) Rottler, J.; Robbins, M. O. *Phys. Rev. E* **2003**, *68*, 011801.

(28) Hoy, R. S.; Robbins, M. O. *Phys. Rev. Lett.* **2007**, *99*, 117801.

(29) Hoy, R. S.; Robbins, M. O. *Phys. Rev. E* **2008**, *77*, 031801.

(30) Rottler, J.; Robbins, M. O. *Phys. Rev. E* **2003**, *68*, 011507.

(31) Pierce, F.; Perahia, D.; Grest, G. S. *Europhys. Lett.* **2011**, *95*, 46001.

(32) Ge, T.; Robbins, M. O.; Perahia, D.; Grest, G. S. manuscript in preparation.

(33) Lacasse, M.-D.; Grest, G. S.; Levine, A. J. *Phys. Rev. Lett.* **1998**, *80*, 309.

(34) Silberberg, A. *J. Colloid Interface Sci.* **1982**, *90*, 86−91.

(35) Theodorou, D. N. *Macromolecules* **1988**, *21*, 1400−1410.

(36) Silberberg, A. *J. Colloid Interface Sci.* **1988**, *125*, 14−22.